OPTICAL REVIEW Vol. 17, No. 2 (2010) 54–60

Endoscopy System for Length Measurement by Manual Pointing with an Electromagnetic Tracking Sensor

Takeshi KOISHI*, Mai SASAKI[1], Toshiya NAKAGUCHI[1], Norimichi TSUMURA[1], and Yoichi MIYAKE[2]

Graduate School of Science and Technology, Chiba University, 1-33 Yayoi-cho, Inage-ku, Chiba 263-8522, Japan
[1]*Graduate School of Advanced Integration Science, Chiba University, 1-33 Yayoi-cho, Inage-ku, Chiba 263-8522, Japan*
[2]*Research Center for Frontier Medical Engineering, Chiba University, 1-33 Yayoi-cho, Inage-ku, Chiba 263-8522, Japan*

(Received July 14, 2009; Revised December 2, 2009; Accepted January 7, 2010)

We propose a practical and simple measurement function of three dimensional (3D) length for endoscopy based on triangulation using manually pointed correspondences. This system is a novel combination of conventional methods. 3D length information is useful for many medical purposes and the burden of manual procedures can be reduced by focusing on length. We employed a novel combination for length measurement, that is, a monocular endoscope with an electromagnetic tracking sensor. The proposed method can measure the length without any equipment for light projection and changing the current procedure of endoscopy. Our method is made more robust and reliable than the automatic correspondence techniques through the best use of the expertise of endoscopists. We developed a prototype system and evaluated its accuracy. From experimental results, we showed that the proposed method can measure the 3D length of static objects accurately as long as the measurement geometry is suitable.

Keywords: endoscopy, endoscope, length measurement, manual pointing, electromagnetic tracking sensor, triangulation

1. Introduction

Endoscopy is widely performed for the diagnosis of the early stage of tumors and the evaluation of the progression and healing of lesions, drug spray, tissue biopsy, and so on. In endoscopy, the size of affected parts is important for deciding a treatment procedure. However, the visual estimation of the size is very difficult even for expert endoscopists owing to the lack of depth information and the distortion caused by wide-angle lenses in endoscopic images.[1)] The quantitative measurement of the size allows more accurate and objective diagnoses, e.g., investigations of tumor growth, ulcer healing, and the effect of antitumor agents, and data collection for statistical analysis.

Many methods for the three dimensional (3D) measurement of endoscopic images were previously proposed. These methods can measure detailed shapes on site easily and rapidly. The methods based on shape-from-shading techniques have been proposed by Deguchi and Okatani.[2)] Many methods based on triangulation have also been proposed. In the triangulation-based methods, the equipment for light projection was often used.[3–7)] The triangulation tends to be more robust and reliable than the shape-from-shading techniques.

In this study, we focused on methods that do not require the equipment for light projection. The examples of this method are proposed by several research groups.[8–11)] However, it is difficult to automatically detect correspondence points required for triangulation owing to indistinctive features and similar colors and textures in an endoscopic image. In our preliminary experiment, few true corresponding points were acquired even using the SIFT detector,[12)] which is known as one of the best performing algorithms.

*E-mail address: takeshi.koishi@gmail.com

In this paper, we propose a practical and simple measurement function of 3D length for endoscopy using manually pointed correspondences. This system is a novel combination of conventional methods. "3D length" is used for distinguishing it clearly from the length in the image (the distance from pixel to pixel). We also employed a novel combination for length measurement, that is, a monocular endoscope with a minute electromagnetic (EM) position-tracking sensor. 3D length information is useful for investigating of tumor growth, ulcer healing, and the effect of antitumor agents.[10)] By focusing on only length, neither area nor volume, the burden of manual procedures can be reduced. Our method is made more robust and reliable than the automatic correspondence techniques through the best use of the expertise of endoscopists. We developed a prototype system using the proposed method and evaluated its accuracy. From experimental results, we showed that the proposed method can measure the 3D length of static objects accurately as long as the measurement geometry is suitable.

2. Methods

Our prototype consists of an endoscope, an EM sensor (Ascension Technology microBIRD), a conventional PC, and a mouse.

2.1 System overview

The flowchart of the proposed system is shown in Fig. 1. First, two frames of the target are captured using an endoscope. The screenshot of this prototype is shown in Fig. 2. The lens distortions of these frames are corrected. An endoscopist selects the target length by determining the start and end points (points A and B in the Fig. 1) in both two frames. Totally, four points are selected. The six-degree-of-freedom (DOF) pose of the endoscope is also acquired using the EM sensor attached to the tip of the endoscope.

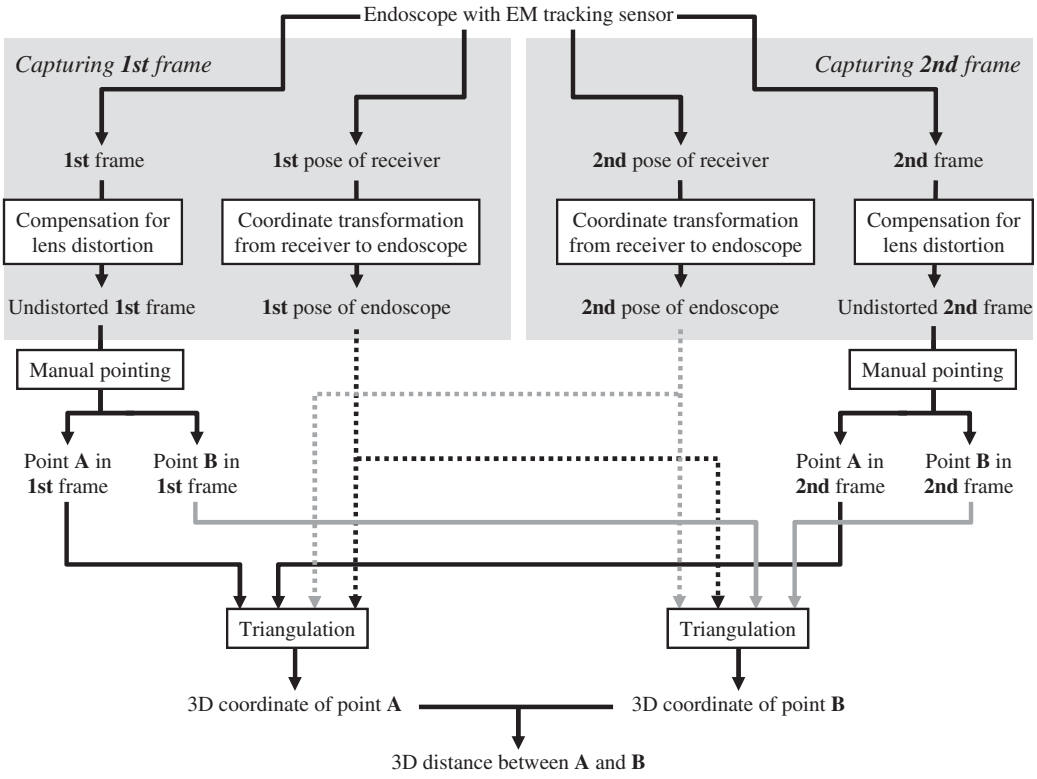

Fig. 1. Flowchart of the proposed system.

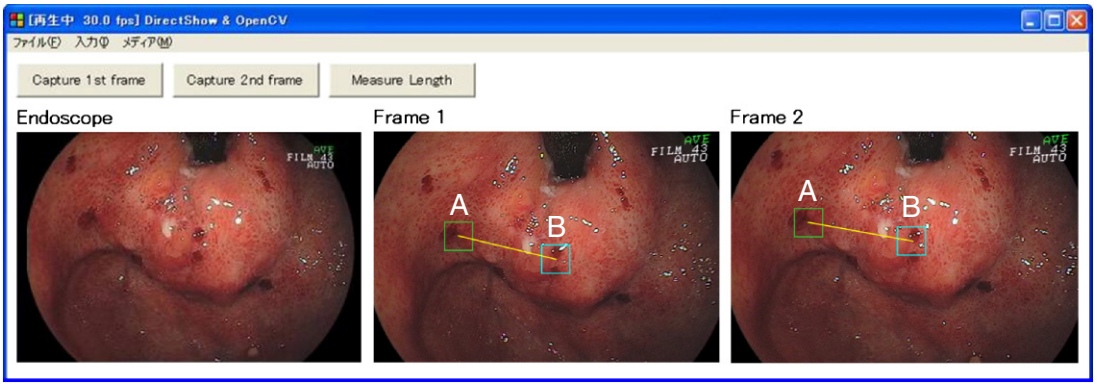

Fig. 2. (Color online) Screenshot of the prototype system. The line segments in the captured frames are the target lengths. The start and end points are in the center of the squares.

Each 3D position on points A and B is calculated by triangulation. Finally, the target length is calculated from the two positions. The targets are the two segment lengths in the captured frames. The start and end points are in the center of the squares.

In this flowchart, the lens distortions of the captured frames are corrected, and then, the frames are displayed. However, some endoscopists may prefer the original distorted frame to the undistorted frame. In this case, another flow can be possible. For example, the captured frames are displayed with lens distortions. The effects of such distortions are considered when 3D positions are calculated.

2.2 *Camera model*

We adopted the camera model implemented in OpenCV[13] for calibrating an endoscope. This camera model is the so-called pinhole camera model that considers a lens distortion. In the pinhole camera model, a scene view is formed by projecting 3D points into the image plane using perspective transformation as

$$s\boldsymbol{m} = \boldsymbol{A}[\boldsymbol{R} \mid \boldsymbol{t}]\boldsymbol{M}, \tag{1}$$

where $\boldsymbol{M} = [X, Y, Z, 1]^{\mathrm{t}}$ is a vector of a 3D point in the world coordinate space, $\boldsymbol{m} = [u, v, 1]^{\mathrm{t}}$ is a point projected from this 3D point into the image plane, s is a scale factor, $\boldsymbol{R}$ is a rotation matrix, and $\boldsymbol{t}$ is a 3D translational vector. The joint

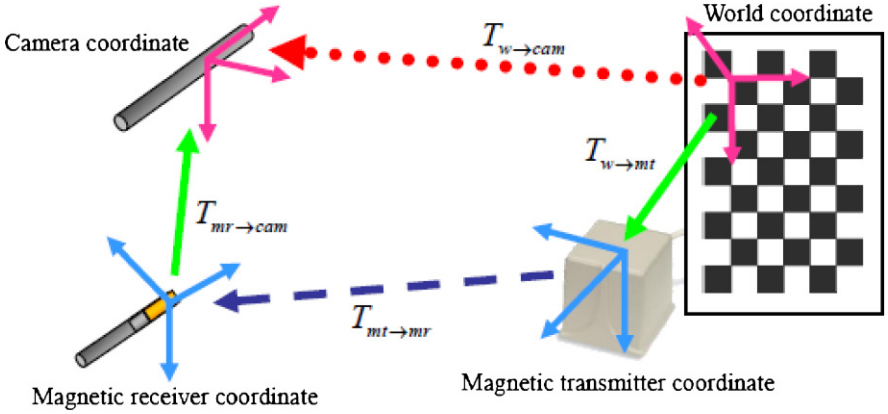

Fig. 3. (Color online) Rigid transformations between the coordinates of the endoscope and electromagnetic tracking sensor.

rotation-translation matrix $[\boldsymbol{R} \mid \boldsymbol{t}]$ indicates extrinsic parameters. $\boldsymbol{A}$ is a matrix of intrinsic parameters given as

$$\boldsymbol{A} = \begin{bmatrix} f_x & 0 & c_x \\ 0 & f_y & c_y \\ 0 & 0 & 1 \end{bmatrix}, \tag{2}$$

where (c_x, c_y) is a principal point (that is typically in the image center). f_x and f_y are focal lengths expressed in pixel-related units. The transformation above is equivalent to (when $z \neq 0$):

$$[x, y, z]^{\mathrm{T}} = \boldsymbol{R}[X, Y, Z]^{\mathrm{T}} + \boldsymbol{t}, \tag{3}$$

$$\begin{cases} u = f_x x' + c_x, & x' = x/z \\ v = f_y y' + c_y, & y' = y/z \end{cases}. \tag{4}$$

These equations express the pinhole camera model without lens distortion. This model was extended for the consideration of the lens distortion as

$$\begin{cases} u = f_x x'' + c_x, \\ \quad x'' = x'(1 + k_1 r^2 + k_2 r^4) + 2p_1 x' y' + p_2(r^2 + 2x'^2) \\ v = f_y y'' + c_y, \\ \quad y'' = y'(1 + k_1 r^2 + k_2 r^4) + p_1(r^2 + 2y'^2) + 2p_2 x' y' \end{cases}, \tag{5}$$

where k_1 and k_2 are radial distortion coefficients. p_1 and p_2 are tangential distortion coefficients. $r^2 = x'^2 + y'^2$. Higher-order coefficients are not considered in OpenCV. The distortion coefficients do not depend on the scene viewed; thus, they are intrinsic camera parameters. They also remain the same regardless of the captured image resolution.

2.3 *Electromagnetic tracking sensor*

The EM tracking sensor consists of the measuring part (receiver) and the origin part (transmitter). The diameter of the receiver is 0.8 mm; thus, the receiver can pass through a channel of an endoscope.

The specific translational error of this sensor is 1.4 mm along each axis of the 3D rectangular coordinate system. The specific angular error is 0.5° in each rotation of the Euler angle. The accuracy of the sensor is degraded by magnetic materials such as metallic objects.

2.4 *Integration of the endoscope and tracking sensor coordinates*

To measure physical positions and orientations, it is required to precisely integrate the coordinate systems of the endoscope and EM tracking sensor. This problem is the so-called hand-eye calibration.[14] In this research, we solved this problem by the following method. This method requires considerable amounts of measured data and processing time, but it can solve this problem.

The rigid transformations between the coordinate systems are shown in Fig. 3. The endoscope-pose $\boldsymbol{T}_{\mathrm{w}\to\mathrm{cam}}$ shown by a dotted arrow cannot be directly measured. Therefore, $\boldsymbol{T}_{\mathrm{w}\to\mathrm{cam}}$ is calculated from the other transformations,

$$\boldsymbol{T}_{\mathrm{w}\to\mathrm{cam}} = \boldsymbol{T}_{\mathrm{mr}\to\mathrm{cam}} \boldsymbol{T}_{\mathrm{mt}\to\mathrm{mr}} \boldsymbol{T}_{\mathrm{w}\to\mathrm{mt}}. \tag{6}$$

The dashed arrow denotes dynamically changeable transformations $\boldsymbol{T}_{\mathrm{mt}\to\mathrm{mr}}$ obtained using the sensor receiver. The transformations $\boldsymbol{T}_{\mathrm{mr}\to\mathrm{cam}}$ and $\boldsymbol{T}_{\mathrm{w}\to\mathrm{mt}}$ are fixed and shown by solid arrows. $\boldsymbol{T}_{\mathrm{mr}\to\mathrm{cam}}$ is fixed by attaching the receiver to the endoscope. About $\boldsymbol{T}_{\mathrm{w}\to\mathrm{mt}}$, the sensor transmitter is fixed on a calibration board, which has a checker pattern also used for camera calibration.

The integration process consists of three steps. The first step is manually obtaining the $\boldsymbol{T}_{\mathrm{w}\to\mathrm{mt}}$ transformation. The second step is estimating $\boldsymbol{T}_{\mathrm{mr}\to\mathrm{cam}}$ by measuring $\boldsymbol{T}_{\mathrm{w}\to\mathrm{cam}}$ and $\boldsymbol{T}_{\mathrm{mt}\to\mathrm{mr}}$. $\boldsymbol{T}_{\mathrm{w}\to\mathrm{cam}}$ can be measured by capturing the checker pattern on the calibration board in the same manner as camera calibration. $\boldsymbol{T}_{\mathrm{mt}\to\mathrm{mr}}$ can be measured using the tracking sensor. In the final step, the preliminary obtained $\boldsymbol{T}_{\mathrm{w}\to\mathrm{mt}}$ and $\boldsymbol{T}_{\mathrm{mr}\to\mathrm{cam}}$ are refined by globally minimizing the reprojection error as

$$\sum_{i=1}^{m} \sum_{j=1}^{n} \| \boldsymbol{T}_{\mathrm{mr}\to\mathrm{cam}} \boldsymbol{T}_{\mathrm{mt}\to\mathrm{mr},i} \boldsymbol{T}_{\mathrm{w}\to\mathrm{mt}} \boldsymbol{x}_{i,j} - \boldsymbol{T}_{\mathrm{w}\to\mathrm{cam},i} \boldsymbol{x}_{i,j} \|^2, \tag{7}$$

where m is the number of captured images, n is the number of corners of the checker pattern, $\boldsymbol{T}_{\mathrm{mt}\to\mathrm{mr},i}$ is the measured pose of the sensor receiver in the i-th image, $\boldsymbol{T}_{\mathrm{w}\to\mathrm{cam},i}$ is the extrinsic parameter of the endoscope in the i-th image, and $\boldsymbol{x}_{i,j}$ are the 3D world coordinates of the j-th corner of the checker pattern in the i-th image.

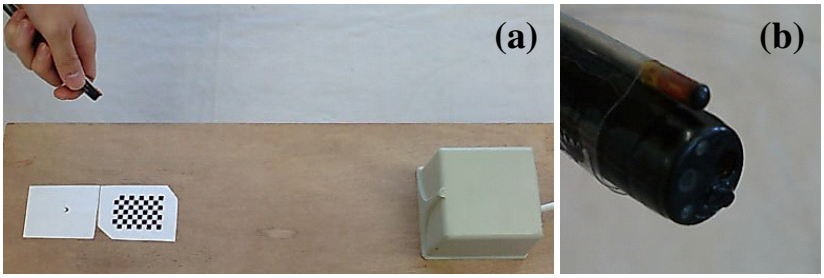

Fig. 4. (Color online) Scene of the experiment for evaluating the proposed method. (a) Scene of the experiment using the endoscope with the tracking sensor. (b) Sensing part (receiver) of the electromagnetic tracking sensor attached to the endoscope.

2.5 *Triangulation*

Triangulation is well known as the method of 3D measurement.[19] We calculated the 3D position by the following algorithm. The projection matrix of the endoscope shown in eq. (1) is substituted as $\boldsymbol{A}[\boldsymbol{R} \mid \boldsymbol{t}]\boldsymbol{M} = \boldsymbol{Q}$. The element of the matrix $\boldsymbol{Q}$ in the i-th row and j-th column is expressed as q_{ij}. At this time, we can write

$$\boldsymbol{BM} = \boldsymbol{b}, \tag{8}$$

$$\boldsymbol{B} = \begin{bmatrix} uq_{31} - q_{11} & uq_{32} - q_{12} & uq_{33} - q_{13} \\ vq_{31} - q_{21} & vq_{32} - q_{22} & vq_{33} - q_{23} \\ u'q'_{31} - q'_{11} & u'q'_{32} - q'_{12} & u'q'_{33} - q'_{13} \\ v'q'_{31} - q'_{21} & v'q'_{32} - q'_{22} & v'q'_{33} - q'_{23} \end{bmatrix},$$

$$\boldsymbol{b} = [q_{14} - uq_{34}, q_{24} - vq_{34}, q'_{14} - u'q'_{34}, q'_{24} - v'q'_{34}]^{\mathrm{T}},$$

where prime represents another pose of the endoscope. Then, the 3D position can be calculated using $\boldsymbol{M} = \boldsymbol{B}^{+}\boldsymbol{b}$ ($+$ represents the pseudo-inverse matrix of $\boldsymbol{B}$).

3. Accuracy Evaluation

We evaluated the accuracy of the proposed method by actual measurement because we consider the practicality important. We investigated the impacts of the following practical error sources: 1) the camera parameters, 2) the specific error of the EM sensor, 3) the error of the integration of the endoscope and tracking sensor coordinates, and 4) the accuracy of the corresponding position by manual pointing.

The scene of the experiment is shown in Fig. 4(a). Although the sensing part of the sensor is attached to the outer surface of the endoscope in the experiment, as shown in Fig. 4(b), this part is sufficiently small to be inserted through the channel of the endoscope.

In our system, an endoscopist is required to specify the corresponding positions manually for triangulation. We assumed that the judgment of the endoscopist is reliable, and consider only the error of the pointing action. However, the pointing error is difficult to be modeled by experiment, because it is affected by many factors, such as types of interface, image size, image resolution, target size, distance to a target, movement time, and differences among endoscopists. Therefore, we did not use the actual measured data with respect only to the manual pointing action. We used a Gaussian distribution to easily model the pointing error, since previous works showed that the spread of hits in rapid aimed movements forms a Gaussian distribution about the target center.[15–17] We can suitably determine how much the pointing error affcts the measurement error using this pointing error model.

3.1 *Experimental condition*

3.1.1 *Calibration*

In the experiment, we first calibrate the endoscope whose image resolution is 720×480 using GML C++ Camera Calibration Toolbox,[18] which is implemented with OpenCV. We use the planar board with a checker pattern which contains 10×7 squares. The size of each square is $5 \times 5\,\mathrm{mm}^2$. This board is observed using the endoscope in 41 poses at a distance of 90–220 mm from the board. The obtained intrinsic parameters are

$$\boldsymbol{A} = \begin{bmatrix} 749.399 & 0 & 357.823 \\ 0 & 674.447 & 215.098 \\ 0 & 0 & 1 \end{bmatrix} \text{pixels},$$

$$k_1 = -0.426024,\ k_2 = 0.165926,$$

$$p_1 = -0.000792,\ p_2 = -0.000654.$$

The average values of the reprojection error are $[0.19, 0.18]$ pixels. Then, the coordinates of the endoscope and EM sensor are integrated by the method mentioned in §2.4. In the experiment, the EM sensor shows only the specific error in the experiments since we remove metallic objects from the experimental environment. The images used for coordinate integration are the same as those used for the camera calibration. The average residual error is 1.12 mm after this coordinate integration.

3.1.2 *Geometry and target of measurement*

The impact of the accuracy of the corresponding positions varies depending on the geometry of triangulation,[19] namely, the pose of an endoscope. We selected five typical poses and called them after their optical axis geometries as *Straight*, *Parallel (Near)*, *Parallel (Far)*, *Cross (Near)*, and *Cross (Far)*. The selected poses are shown in Fig. 5. These poses cover the accuracy stability of triangulation to the detection accuracy of the corresponding points. The *Straight* pose is the most sensitive to the accuracy of the corresponding positions. This pose is used in the examination of narrow organs, such as an esophagus and a duodenum. The *Parallel*

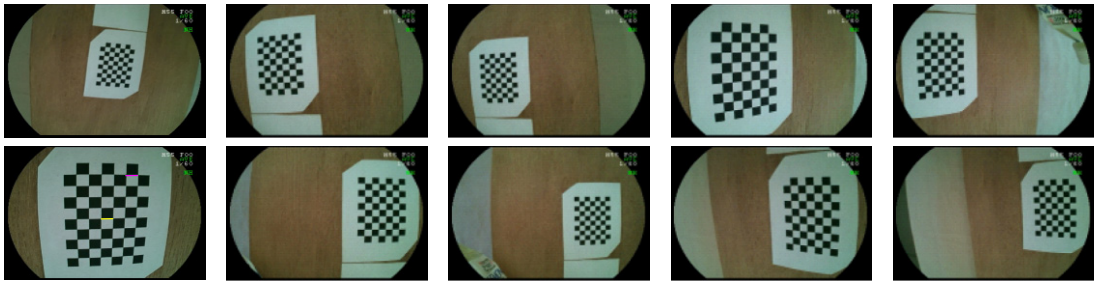

(a) (b) (c) (d) (e)

Fig. 5. (Color online) Geometries of triangulation used in the evaluation experiment. These geometries are called after each optical axis geometry in this paper. (a) Straight. (b) Parallel (Near). (c) Parallel (Far). (d) Cross (Near). (e) Cross (Far).

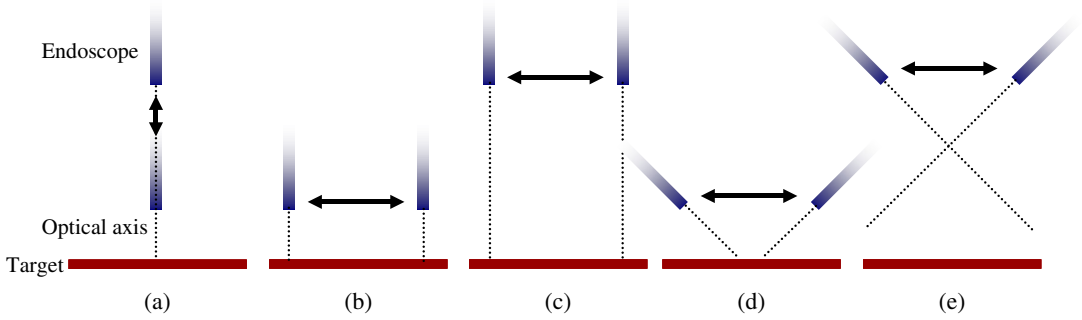

Fig. 6. (Color online) Captured images of the line segments measured at the selected geometries. The measured line segments are indicated in yellow and pink. The pink line is used for evaluating the impact of the distance from a measured object to the optical axis of the endoscope. (a) Straight. (b) Parallel (Near). (c) Parallel (Far). (d) Cross (Near). (e) Cross (Far).

pose is the most popular in the stereovision because of its relatively low sensitivity to the accuracy of the corresponding positions and its suitability for the automatic detection of the corresponding positions. In both cases of straight and parallel poses, the sensitivity to the accuracy of the corresponding positions increases as the baseline becomes shorter. The *Cross* pose is the most robust to the error of the corresponding positions. The distance to a measurement target is related to the image resolution in all the cases. The evaluation of the rotation about the optical axis is unnecessary because the rotation about the optical axis does not change the accuracy of the triangulation.

In addition to the pose of an endoscope, the distance from a measurement target to the optical axis of the endoscope is also related to the sensitivity to the accuracy of the corresponding positions. The effect of this distance is smaller than that of the pose of the endoscope. Therefore, we perform an experiment on this distance only when the pose of the endoscope is straight, because the effect of this distance becomes much larger than those for the other poses.

We measured a 5-mm-long line segment, which is a part of the checker pattern used for the calibration process. By using the checker pattern, we can not only examine the total error but also estimate the pose of the endoscope with the EM sensor by comparison with the pose accurately calculated by the camera calibration technique. This line segment is captured at the selected geometries of triangulation. The captured images are shown in Fig. 6. The measured line segments are indicated in yellow and pink. The pink line is used for evaluating the impact of the distance from a measured object to the optical axis of the endoscope.

3.1.3 *Error model of manual pointing*

We use a Gaussian distribution to easily model the pointing error. When the true image coordinates of the target point are (u, v), the manually pointed image coordinate $(\hat{u}, \hat{v})$ can be described as

$$\hat{u} = u + \Delta u_{\mathrm{nr}}, \ \hat{v} = v + \Delta v_{\mathrm{nr}}, \tag{9}$$

where Δu_{nr} and Δv_{nr} are the pseudo-random numbers that form the Gaussian distributions whose mean is 0 and variance is σ^2. Then, the pointed image coordinate is rounded to an integer coordinate due to the quantization caused by the limits of image resolution. Therefore, the pointing error $(\Delta u, \Delta v)$ is

$$\Delta u = \lfloor \hat{u} + 0.5 \rfloor - u, \ \Delta v = \lfloor \hat{v} + 0.5 \rfloor - v. \tag{10}$$

This error model is used for accuracy evaluation.

In this study, three values, namely, 0.5, 1.0, and 2.0 pixels, are used as the standard deviations of this model. The pointing error within 2 pixels is empirically easy to be achieved with a conventional mouse. We generate one-million pointing data and calculate the RMSE value in each case for evaluation.

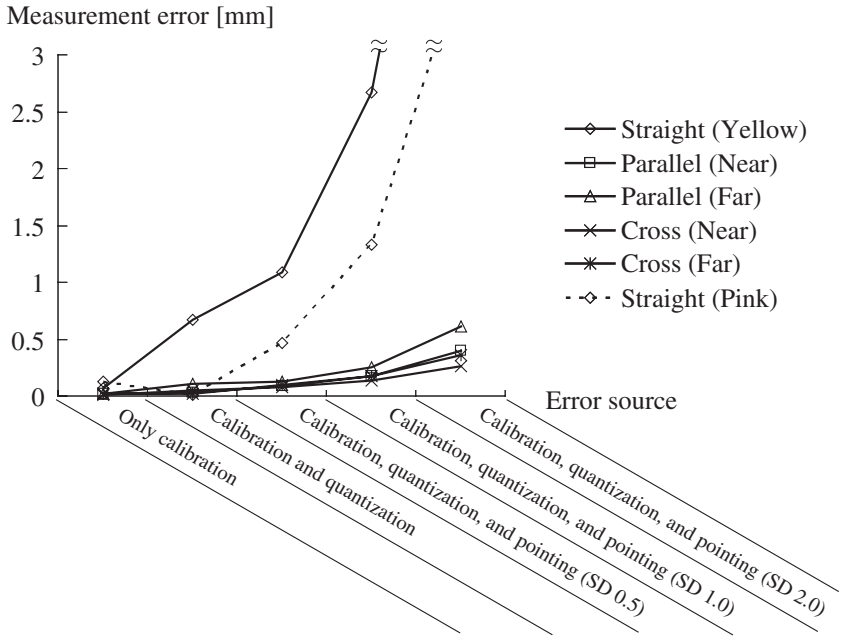

Fig. 7. Measurement error of the 5-mm-long line segment without the EM sensor. The horizontal axis is an error source: "Only calibration", "Calibration and quantization", "Calibration, quantization, and pointing". "Calibration" is camera calibration. "Quantization" is caused by the limits of the image resolution. The error of "Pointing" is given by the error model whose standard deviation is set to 0.5, 1.0, and 2.0 pixels. In the case considering the pointing error, the RMSE value is plotted in this graph.

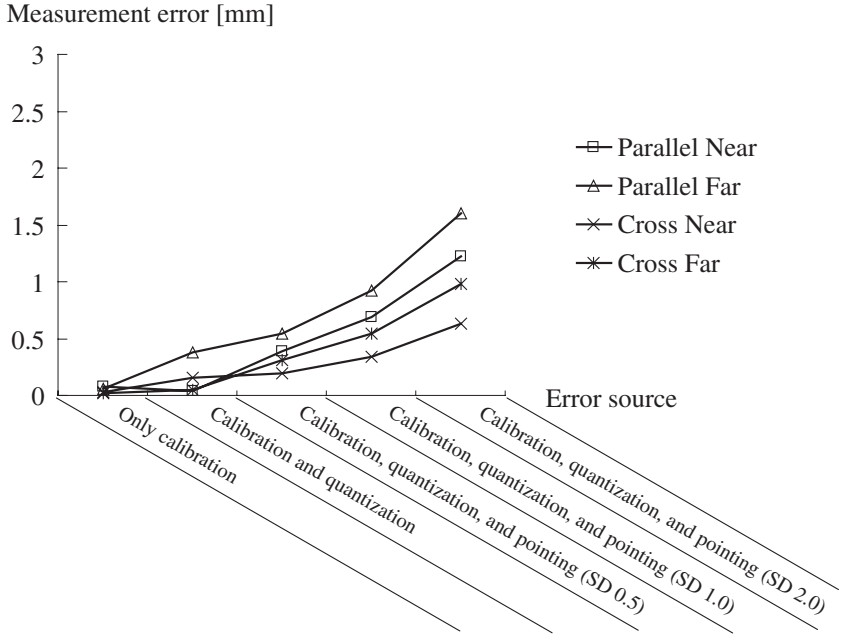

Fig. 8. Measurement error of the 5-mm-long line segment obtained using the EM sensor.

3.2 Results

First, the measurement error without the EM sensor is shown in Fig. 7. The error larger than 3 mm (60% of the target length of 5 mm) is not plotted in this figure, because we consider that the 3 mm error is equal to or more inaccurate than value estimated by endoscopists. This criterion is based on the following two results in ref. 1: the estimated results were $-29 \pm 40\%$ relative to the true square of the ulcers and the deviation value did not depend on the shape of the ulcers.

We found that the effect of the camera calibration error is sufficiently small. Also, the error at the straight pose is much larger than those at the other poses. The impact of the pose of the endoscope is higher than that of the pointing error.

When the RMSE of the yellow line segment is compared with that of the pink one at the straight pose (the colors of the line segments are shown in Fig. 6), the impact of the pose is also higher than that of the distance from the line segment to the optical axis of the endoscope. Next, the measurement error using the EM sensor is shown in Fig. 8. We found that the pattern is similar to that in Fig. 7. However, the accuracy slightly decreases owing to the errors of the EM sensor itself and its coordinate integration with the endoscope. All the errors in the case of the straight pose are greater than 4 mm. These results indicate that we can measure the length accurately by setting a suitable endoscope pose.

4. Discussion

The proposed method can measure the 3D length of static objects robustly and reliably without changing the current procedure of endoscopy. We also showed that the proposed method can measure the length accurately as long as the measurement geometry is suitable. We should investigate the limit of the baseline length for realizing an acceptable accuracy.

The purpose of this study is to evaluate the effects of the following factors on the measurement accuracy: camera calibration, a specific error of the EM sensor, integration of the endoscope and sensor coordinates, measurement geometry, and the corresponding position. For practical use, we should also address the effects of the magnetic distortion caused by metallic objects. This distortion can be calibrated by introducing the methods proposed by several research groups[20,21] to our system. The motion of an organ also degrades the measurement acuuracy, because the proposed method uses temporally continuous two frames of a monocular endoscope. Although this problem can be eliminated by using a stereoscopic endoscope with a sufficient baseline length between two cameras, the stereoscopic endoscope becomes much thicker than the monocular one. Therefore, we must develop an algorithm estimating the deformation of organs for monocular measurement.

We have a plan to improve the pointing interface of the proposed method. The accuracy may be improved by enlarging the captured frame of the endoscopic image sequence for display. In addition to the size of the displayed image, a suitable pointing interface other than the normal mouse will be introduced.

Moreover, we would like to establish the error model of all the error sources of the measurement system for more detailed analysis and optimal system design in addition to actual measurements.

5. Conclusions

We propose a practical and simple measurement function of 3D length using manually pointed correspondences and a monocular endoscope with an EM tracking sensor. This system is a novel combination of conventional methods. Our method is made more robust and reliable than the automatic correspondence techniques through the best use of the expertise of endoscopists. 3D length information is useful for many medical purposes and the burden of manual procedures can be reduced by focusing on length. The proposed method can measure the length without any equipment for light projection and changing the current procedure of endoscopy. We developed a prototype system and evaluated its accuracy. From experimental results, we showed that the proposed method can measure the 3D length accurately as long as the measurement geometry is suitable. In the future, we intend to improve the proposed method for practical use.

Acknowledgment

We would like to thank Professor Tatsuo Igarashi (CFME at Chiba University), Professor Hideki Hayashi (CFME at Chiba University), and Mr. Yoshimichi Okada (Chiba University) for their comments and help in our experiments.

References

1) A. Sonnenberg, M. Giger, L. Kern, C. Noll, K. Stuby, K. B. Weber, and A. L. Blum: Br. Med. J. **2** (1979) 1322.
2) K. Deguchi and T. Okatani: Proc. IEEE/SIAM Joint Workshop Mathematical Methods in Biomedical Image Analysis, 1996, p. 290.
3) H. Haneishi, T. Ogura, and Y. Miyake: Opt. Lett. **19** (1994) 601.
4) K. Hasegawa, K. Noda, and Y. Sato: Proc. Int. Conf. Pattern Recognition, 2002, p. 792.
5) D. Yelin, I. Rizvi, W. M. White, J. T. Motz, T. Hasan, B. E. Bouma, and G. J. Tearney: Nature **443** (2006) 765.
6) M. Chan, W. Lin, C. Zhou, and J. Y. Qu: Appl. Opt. **42** (2003) 1888.
7) H. Nakatani, K. Abe, A. Miyakawa, and S. Terakawa: J. Biomed. Opt. **12** (2007) 051803.
8) N. Oda, J. Hasegawa, T. Nonami, M. Yamaguchi, and N. Ohyama: Opt. Rev. **2** (1995) 110.
9) K. Deguchi, T. Sasano, H. Arai, and H. Yoshikawa: IEICE Trans. Inf. Syst. **E79-D** (1996) 1329.
10) K. Yao, T. Matsui, H. Furukawa, T. Yao, T. Sakurai, and T. Mitsuyasu: Gastrointest. Endosc. **55** (2002) 412.
11) D. Koppel, C.-I. Chen, Y.-F. Wang, H. Lee, J. Gu, A. Poirson, and R. Wolters: Proc. SPIE **6509** (2007) 65091L.
12) D. G. Lowe: Int. J. Comput. Vision **60** (2004) 91.
13) G. Bradski and A. Kaebler: *Learning OpenCV* (O'Reilly, Sebastopol, CA, 2008).
14) R. Horaud and F. Dornaika: Int. J. Robot Res. **14** (1995) 195.
15) T. Grossman and R. Balakrishnan: ACM Trans. Comput.–Hum. Interaction **12** (2005) 435.
16) J. O. Wobbrock, E. Cutrell, S. Harada, and I. S. MacKenzie: Proc. 26th Annu. SIGCHI Conf. Human Factors in Computing Systems, 2008, p. 1613.
17) S. Zhai, J. Kong, and X. Ren: Int. J. Hum.–Comput. Stud. **61** (2004) 823.
18) V. Vezhnevets and A. Velizhev: GML C++ Camera Calibration Toolbox (2005) [http://research.graphicon.ru/calibration/gml-c++-camera-calibration-toolbox.html].
19) R. Hartley and A. Zisserman: *Multiple View Geometry in Computer Vision* (Cambridge University Press, Cambridge, U.K., 2003).
20) M. Nakamoto, K. Nakada, Y. Sato, K. Konishi, M. Hashizume, and S. Tamura: IEEE Trans. Med. Imaging **27** (2008) 255.
21) M. Feuerstein, T. Reichl, J. Vogel, A. Schneider, H. Feussner, and N. Navab: Proc. Medical Image Computing and Computer-Assisted Intervention, 2007, LNCS 4791, p. 458.